

Forecasting the extreme rainfall, low temperatures, and strong winds associated with the northern Queensland floods of February 2019



T. Cowan^{a,b,*}, M.C. Wheeler^b, O. Alves^b, S. Narsey^b, C. de Burgh-Day^b, M. Griffiths^b, C. Jarvis^a, D.H. Cobon^a, M.K. Hawcroft^{a,c}

^a Centre of Applied Climate Science, University of Southern Queensland, Toowoomba, Queensland, Australia

^b Bureau of Meteorology, Melbourne, Victoria, Australia

^c Met Office, Exeter, United Kingdom

ARTICLE INFO

Keywords:

Extreme
Rainfall
Temperature
Flood
Forecast
Skill
Madden-Julian Oscillation
Subseasonal

ABSTRACT

From late January to early February 2019, a quasi-stationary monsoon depression situated over northeast Australia caused devastating floods, killing an estimated 625,000 head of cattle in northwest Queensland, and inundating over 3 000 homes in the coastal city of Townsville. The monsoon depression lasted ~10 days, driving daily rainfall accumulations exceeding 200 mm/day, maximum temperatures 8–10 °C below normal, and wind gusts above 70 km/h. In this study, the atmospheric conditions during the event and its predictability on the weekly to subseasonal range are investigated. Results show that during the event, the tropical convective signal of the Madden-Julian Oscillation was over the western Pacific, and likely contributed to the heavy rainfall, however the El Niño-Southern Oscillation was not in the usual phase for increased rainfall over Queensland. Over the northern Tasman Sea, an anticyclone helped maintain a positive phase of the Southern Annular Mode and promote onshore easterly flow. Somewhat consistent with these climate drivers, the monthly rainfall outlook for February issued by the Australian Bureau of Meteorology on 31 January provided no indication of the event, yet forecasts, not available to the public, of weekly-averaged conditions by the Bureau's dynamical subseasonal-to-seasonal (S2S) prediction system were more successful. For the week of 31 January to 6 February the prediction system forecast a more than doubling of the probability of extreme (highest quintile) weekly rainfall a week prior to the event, along with increased probabilities of extremely low (lowest quintile) maximum temperatures and extreme (highest quintile) wind speeds. Ensemble-mean weekly rainfall amounts, however, were considerably underestimated by the prediction system, even in forecasts initialised at the start of the peak flooding week, consistent with other state-of-the-art dynamical S2S prediction systems. Despite this, one of the individual ensemble members of the Bureau's prediction system did manage to forecast close to 85% of the magnitude of the rainfall across the most heavily impacted region of northwest Queensland a week before the event. Predicting this exceptional event beyond two weeks appears beyond our current capability despite the dynamical system forecasts showing good skill in forecasting the broad-scale atmospheric conditions north of Australia a week prior.

1. Introduction

From late January to early February 2019, northern Queensland faced over a week of extreme rainfall, relatively low maximum temperatures, and wind gusts in excess of 70 km/h (Figs. 1 and 2, Supplementary Tables S1 and S2). Subsequent flooding caused significant infrastructure damage, and compounded by the extreme wind chill, led to the deaths of an estimated 625,000 head of cattle and 48,000 sheep

across northwest Queensland (<https://www.queenslandcountrylife.com.au/story/6186448/elation-turns-to-despair-in-the-north-west/>; last accessed 31/05/2019), as well as extensive inundation to Townsville along the northeast coast (Gissing et al., 2019). Satellite imagery taken soon after the event shows the aftermath of flood waters that ended up covering an area of approximately 200,000 km², primarily in the catchments of the Flinders, Burdekin, and Diamantina rivers (Fig. 3). This was caused by a quasi-stationary monsoon depression, bringing

* Corresponding author. Centre of Applied Climate Science, University of Southern Queensland, Toowoomba, Queensland, Australia.

E-mail address: tim.cowan@bom.gov.au (T. Cowan).

<https://doi.org/10.1016/j.wace.2019.100232>

Received 1 June 2019; Received in revised form 30 September 2019; Accepted 1 October 2019

Available online 2 October 2019

2212-0947/Crown Copyright © 2019 Published by Elsevier B.V. This is an open access article under the CC BY-NC-ND license

(<http://creativecommons.org/licenses/by-nc-nd/4.0/>).

over 600 mm of rainfall during a 10-day period to many inland locations (Bureau of Meteorology, 2019b). The depression developed on the back of a delayed monsoon onset over northern Australia and record hot conditions from November 2018 to January 2019 (Bureau of Meteorology, 2019a). This sudden switch from hot and dry to wet and cool reportedly contributed to the impact of the event in terms of livestock losses (M. Munchenberg, Pers. Comms.).

Unfortunately, the official monthly rainfall outlook issued by the Bureau of Meteorology on 31 January for February provided little indication that the affected region of northern Queensland would be so anomalously wet, even though much of the extreme rainfall occurred in the first week of February. For northwest Queensland the outlook indicated only a 45–55% chance of exceeding the median monthly rainfall, and over Townsville, a 35–40% chance (Fig. 4). The same outlook also indicated less than a 15% chance of at least 300 mm for all of February over most of the affected region (not shown). This outlook was based on dynamical model forecasts that were initialised from 18–26 January with the Australian Community Climate Earth-System Simulator – Seasonal version 1 (ACCESS-S1). At the time, practice at the Bureau involved climatologists spending up to 5 days generating products and examining the model forecasts before a monthly or seasonal outlook was publicly issued (this is now down to 3 days).

This event therefore raises several important questions:

- 1) What were the large-scale climate conditions that may have contributed to this extreme event?
- 2) Why did the Bureau of Meteorology's issued monthly outlook for February seem to miss the event?
- 3) Would a forecast product that was targeted to the multi-week time scale, and issued within a day of being generated, have provided greater benefit?

In this study we attempt to answer these questions by first describing in more detail, the observed conditions during the extreme event, and second, examining the associated meteorology and large-scale climate drivers acting at the time of this event. We focus on the interannual and intra-seasonal modes of climate and weather variability and discuss their potential role in this event.

Third, we investigate the predictability of this event in weekly-averaged forecasts from ACCESS-S1: the Bureau's newest subseasonal to seasonal (S2S) dynamical prediction system, the same system that was used to generate the monthly outlook described earlier. We look in detail at forecasts that target the week of 31 January to 6 February, hereafter defined as the *peak week* of the event. We therefore investigate whether there was improved predictability on a multi-week scale. This event is an ideal test case because of its duration of around 7–10 days. Although such multi-week forecasts were not publicly available at the time of the event, this study serves to demonstrate and verify the kind of forecast products that may be publicly released in the future.

Finally, we provide a comparison of ACCESS-S1 to other modern S2S dynamical prediction systems from the international modelling community, to determine if the severity of the event was predictable both across the ensemble means and individual members of each system. This provides further insight as to the predictability of extreme events like this with a 1–2 week lead time.

2. Data and methods

2.1. Observations and reanalysis

Observed rainfall and temperature data are taken from the Bureau of Meteorology's 5 km resolution Australian Water Availability Project (AWAP) gridded datasets (Jones et al., 2009). Complementing this, we utilise weather station data from six of the most heavily impacted regional towns in northwest and central Queensland that experienced wide-spread cattle losses and infrastructure damage (see Table 1 for weather station information and Fig. 3 for approximate locations). Using the 9am and 3pm station temperature observations, we use the method of Steadman (1994) to compute apparent temperatures from the dry bulb temperature, relative humidity, and wind speed. We utilise daily atmospheric fields of mean sea level pressure (MSLP) and 850-hPa winds from the NCEP-NCAR reanalysis 1 (NNR; Kalnay et al., 1996), and Outgoing Longwave Radiation (OLR) from the National Oceanic and Atmospheric Administration's polar-orbiting satellites. Indices of large-scale climate drivers are taken from the research literature and updated where appropriate.

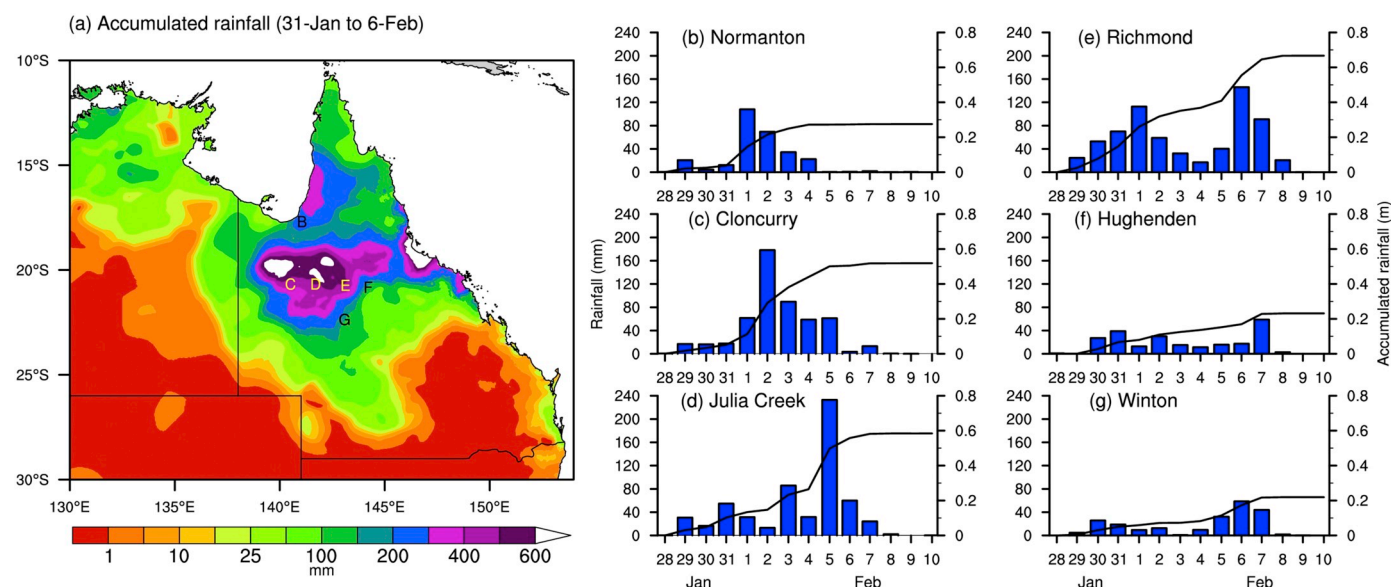


Fig. 1. Precipitation during the February 2019 flooding event. (a) Observed accumulated rainfall over 31 January to 6 February. (b–g) Daily rainfall totals (blue bars) and rainfall accumulations (black lines) at six northwest Queensland stations (see Table 1) from 28 January to 10 February. The stations used for (b–g) are the airports at: Normanton, Cloncurry, Julia Creek, Hughenden and Winton, and the Post Office at Richmond (locations shown in map). Note the 31 January observation for Cloncurry Airport was not taken and is replaced here by the Cloncurry McIlwraith St observation (17.8 mm, ~5 km away). (For interpretation of the references to colour in this figure legend, the reader is referred to the Web version of this article.)

2.2. The Bureau's S2S prediction system

The Bureau of Meteorology's newest dynamical seasonal prediction system, ACCESS-S1, was introduced operationally in 2018 as a replacement for the Predictive Ocean Atmosphere Model for Australia (POAMA; Hudson et al., 2018). The model component of ACCESS-S1 is the same as that used in the UK Met Office Global Seasonal forecast system version 5 (MacLachlan et al., 2015), but the initial conditions have some differences. The model atmosphere has a horizontal resolution of N216 (60 km in the mid-latitudes) and 85 vertical levels. In comparison, POAMA's horizontal resolution was approximately 250 km with 17 vertical levels. The ocean component of ACCESS-S1 has a 0.25° horizontal resolution (approximately 25 km) on a tripolar grid with 75 levels in the vertical. The land surface model (Joint UK Land Environment Simulator; JULES) is made up of four soil levels and is coupled to the atmosphere with the same grid resolution. ACCESS-S1 relies on the Met Office's Forecast Ocean Assimilation Model (FOAM) for its ocean and sea-ice initial conditions, the Bureau's global numerical weather prediction 4D-Var data assimilation analyses for its real-time atmospheric initial conditions, and the ERA-Interim reanalyses (Dee et al., 2011) for its hindcast atmospheric initial conditions. In real time during the period of interest, the ACCESS-S1 system was run daily with 33 ensemble members generated using perturbed initial conditions. Twenty-two of these ensemble members stop after 35 days, and 11 continue for 217 days (~6.5 months).

Here we analyse the real-time multi-week forecasts of ACCESS-S1 for weeks 1, 2, and 3, which are equivalent to lead times of 0, 1, and 2 weeks measured to the start of the event, respectively. These multi-week forecasts are based on a larger 99-member ensemble constructed from the 33 members per day lagged over 3 days (Hudson et al., 2018). For example, the week 2 forecast from the 24 January is targeting the week of 31 January to 6 February and consists of 33-members initialised on each day from 22, 23 and 24 January. For the monthly and seasonal outlooks (e.g. Fig. 4), a 99-member ensemble is constructed from 11 members lagged over 9 days, because only 11 of the original 33 members are run for longer than 35 days (Hudson et al., 2018). The raw precipitation, Tmax and wind speed forecasts from the model are calibrated to a 5 km grid over Australia to match observations, using a

quantile-quantile mapping approach (Jeon et al., 2016). The calibration is trained using the model hindcast ensemble and corresponding observations over 1990-2012. This approach is applied to all locations and lead times, and where the raw forecast data is more extreme than anything occurring in the model training data, the calibrated value is calculated as the raw value multiplied by the ratio of the observed maximum (or minimum) training value to the model maximum (or minimum) training value. This calibration serves to remove model mean biases as well as make the grid scale daily rainfall amounts more realistic. Further details on ACCESS-S1 system's mean-state biases are detailed in Hudson et al. (2018).

For this study we show new prototype products that provide tailored information on the likelihood of extreme weekly conditions over Australia. The prototype suite of products described are experimental and not currently official Bureau of Meteorology products. They were developed as part of the Forewarned is Forearmed project for trial purposes (Hudson et al., 2016), and include both Australia-wide maps and point forecasts, based on the 5 km grid of calibrated output. We show one such prototype product which describes the likelihood of a given forecast week being in the highest or lowest quintile category. We also show the likelihood of extreme high precipitation and low maximum temperature for grid locations closest to the hardest hit regional communities of Julia Creek, Cloncurry, Richmond, Hughenden and Winton. These are among the more than 70 locations over northern Australia used to validate the ACCESS-S1 hindcasts and forecasts. Finally, we analyse forecasts of the weekly precipitation totals, although we emphasise that the purpose of the ACCESS-S1 ensemble is primarily to give an estimation of the possible precipitation distribution.

As part of our assessment we compare ensemble forecasts from four additional coupled prediction systems obtained from the S2S Project database (Vitart et al., 2017). They are those of the European Centre for Medium-Range Weather Forecasts (ECMWF, 2018), NCEP (Saha et al., 2014), Météo-France (Voldoire et al., 2013), and the Bureau's POAMA system (Cottrill et al., 2013). POAMA is on a 2.5° × 2.5° regular latitude-longitude grid, while the three remaining forecast centres provide output on a 1.5° × 1.5° grid. The corresponding ensemble sizes are 51 members for ECMWF and Météo-France, 33 for POAMA, and 16 for NCEP. Both POAMA and ECMWF are initialised twice per week,

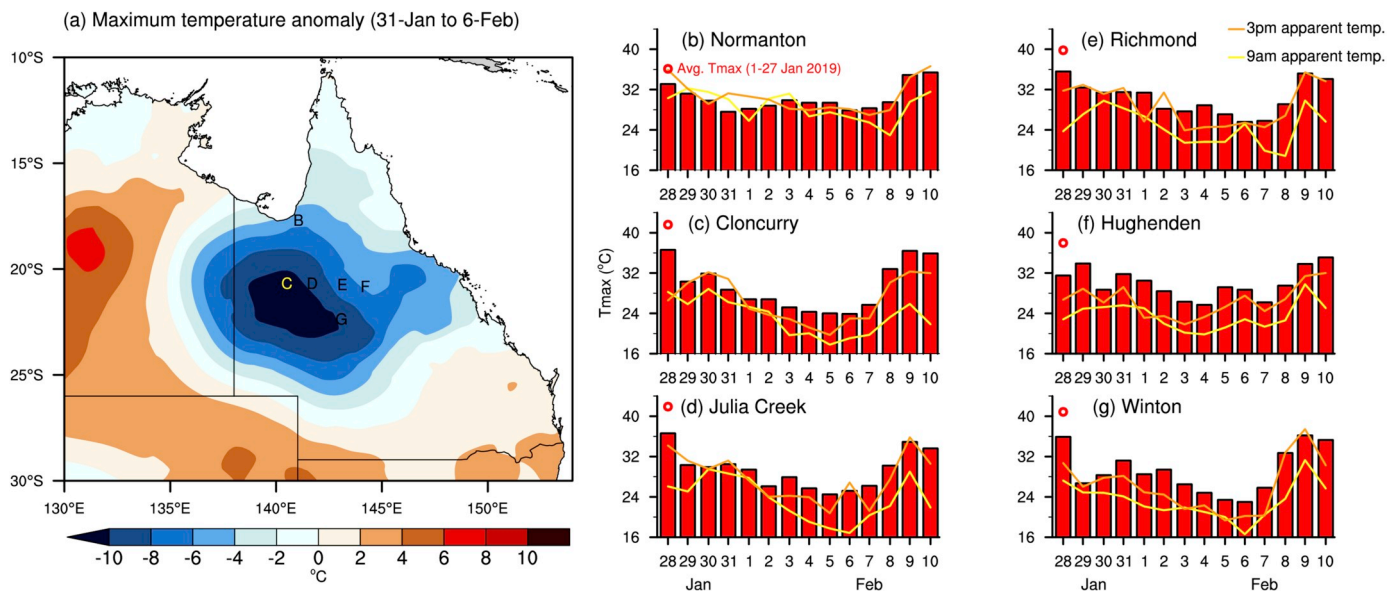


Fig. 2. Mean maximum temperature anomalies during the February 2019 flooding event. (a) Observed maximum temperature anomalies averaged over 31 January to 6 February. Anomalies are calculated with respect to a 1961-1990 climatology. (b-g) Daily maximum temperatures (red bars) and apparent temperatures (yellow = 9am, orange = 3pm) at six northwest Queensland stations (as in Fig. 1) from 28 January to 10 February. The red open circles in (b-g) indicate the average daily maximum temperature for the first 27 days of January 2019. (For interpretation of the references to colour in this figure legend, the reader is referred to the Web version of this article.)



Fig. 3. Real colour satellite image of the extreme flooding event over northern Queensland. The image, taken on 11 February 2019, shows the vast flooded areas (sandy colours), including the river outflows into the Gulf of Carpentaria (upper-left of image) and Coral Sea (right side of image). (For interpretation of the references to colour in this figure legend, the reader is referred to the Web version of this article.)

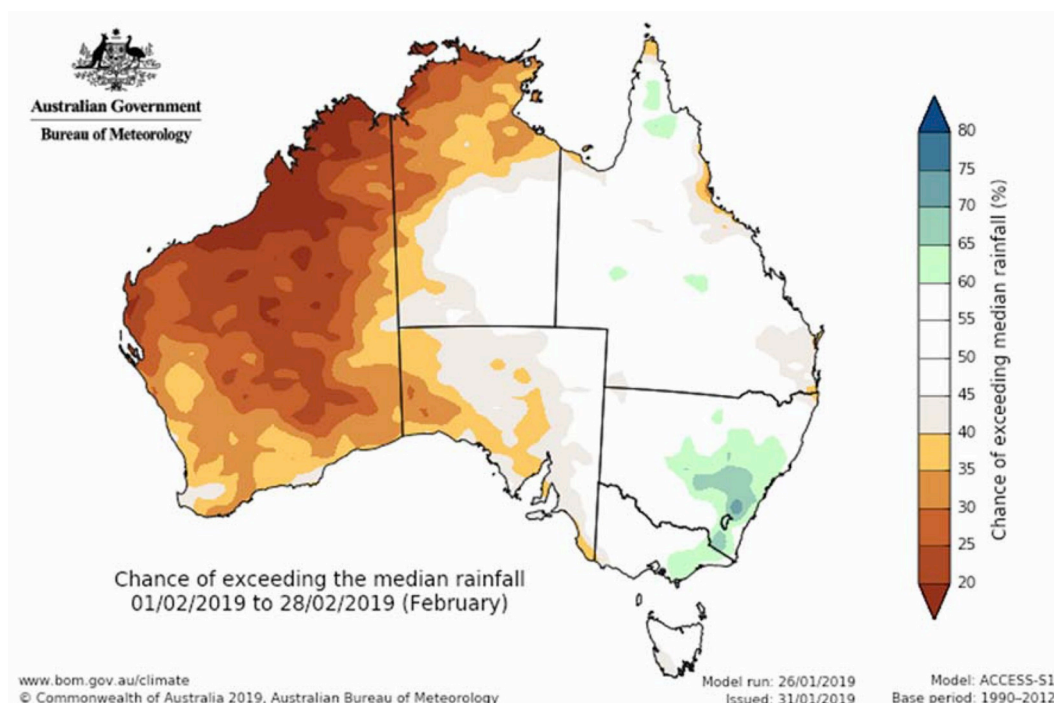


Fig. 4. Rainfall outlook for February 2019 issued by the Bureau of Meteorology on 31 January, showing the chance of exceeding the median February rainfall. The outlook is based on the ACCESS-S1 system’s 99-member lagged forecast ensemble using initial conditions from 18-26 January.

Météo-France once per week, and NCEP daily. These systems share a common forecast initial condition date of 24 January, which we use to examine the forecast target week of 31 January to 6 February. More information on the S2S prediction systems is provided at <https://confluence.ecmwf.int/display/S2S/Models> (last accessed 30/05/2019).

3. Results

3.1. Observed conditions during the event

In the *peak week* of 31 January to 6 February, over 400 mm of rain fell over a large proportion of northwest Queensland and along the north-east coast (Fig. 1a; Supplementary Fig. S1a). For the northwest region, 7-day totals exceeding 500 mm were observed at more than 10 of the Bureau’s standard rain gauge stations (Bureau of Meteorology, 2019b), including Julia Creek Airport with 510.2 mm (Fig. 1d), with 233 mm

Table 1

Coordinates, median rainfall and mean maximum temperature from stations over northwest and central Queensland impacted by the extreme conditions in February 2019. The calculated medians are based on the period 1981-2010 unless listed in square brackets under the station name column. The values listed in the square brackets in the station number column are the distances (in km) between each town's centre and airport. The stations used for the ACCESS-S1 forecast products in Fig. 9 are shown in **bold**.

| Station name | Station number [Distance in km] | Latitude (°S) | Longitude (°E) | Median Feb. rainfall (mm) | Mean Feb. maximum temperature (°C) |
|--|---------------------------------|---------------|----------------|---------------------------|------------------------------------|
| Cloncurry Airport | 029141 | 20.67 | 140.51 | 85.1 | 36.2 |
| Cloncurry McIllwraith St | 029008 [4.9] | 20.71 | 140.52 | 74.4 | - |
| Julia Creek Post Office | 029025 | 20.66 | 141.75 | 103.3 | 36.9 |
| Julia Creek Airport [2002-2018] | 029058 [2.8] | 20.67 | 141.72 | 92.4 | 37.2 |
| Richmond Post Office | 030045 | 20.73 | 143.14 | 76.0 | 36.0 |
| Richmond Airport [1999-2018] | 030161 [4.0] | 20.70 | 143.12 | 73.2 | 36.4 |
| Hughenden Post Office | 030024 | 20.84 | 144.20 | 82.5 | 34.9 |
| Hughenden Airport [2001-2018] | 030022 [4.6] | 20.82 | 144.23 | 51.5 | 35.2 |
| Winton Post Office | 037051 | 22.39 | 143.04 | 58.3 | 36.7 |
| Winton Airport [2003-2018] | 037039 [5.6] | 22.36 | 143.08 | 60.6 | 37.2 |
| Normanton Post Office | 029041 | 17.67 | 141.07 | 191.4 | 34.1 |
| Normanton Airport [2002-2018] | 029063 [1.9] | 17.69 | 141.07 | 169.6 | 33.8 |

falling on a single day (5 February). Other stations including Cloncurry Airport and Richmond Post Office experienced 10-day totals exceeding 500 mm (Fig. 1c,e), while towns on the periphery of the precipitation maxima (e.g., Normanton, Winton and Hughenden) saw 10-day totals above 200 mm. Along the northeast coast, Townsville was severely impacted, with 1400 mm of rainfall falling in a 13-day period from 27 January to 8 February (Supplementary Fig. S1). For stations that have more than 30 years of observations, four set new daily rainfall records for any month of the year, 18 set new 7-day records for any month, and 21 set new 10-day records for any month, including Richmond Post Office (Fig. 1e). This confirms that this event was most extreme at the weekly time scale as opposed to daily. For example, for the first 8 days of February at Townsville Aero (Supplementary Fig. S1b), the 953.4 mm that fell was more than 360 mm above the decile 9 rainfall amount for that month (591.8 mm based on 1981-2010 data).

The spatial and temporal variability of the rainfall associated with the event is highlighted in Fig. 5a, where we see the clear topographical separation of coastal rainfall (e.g., Townsville) to the inland Gulf stations west of the Great Dividing Range. For example, at Hughenden Airport (20.82°S, 144.23°E), only 231.4 mm of rain fell between 28 January and 8 February, with a highest daily total of 58.8 mm on 7

February. In contrast, Julia Creek, 260 km west of Hughenden, experienced 584.2 mm over the same 12-day period. A temporal feature of the inland Gulf stations' rainfall were the two distinct peaks (Fig. 5a): the first, from 1-4 February, was relatively stationary and impacted locations to the west of Cloncurry (139°-140.5°E). The second occurred from 5-7 February and affected regions east of Cloncurry to Richmond (143.1°E). This event slowly migrated eastwards over the three days, inundating Julia Creek on 5 February (233 mm), Richmond on the 6-7 February (146 and 91 mm, respectively) and Hughenden on 7 February (59 mm). Along the east coast, however, the rainfall was more continuous (see Supplementary Fig. S1b).

As the monsoon depression migrated inland from the Gulf, maximum temperatures quickly dropped from around 40 °C in late January to below 27 °C from 3 February, with anomalies in the peak week between 6 °C and 10 °C below the 1961-1990 weekly average (Fig. 2a). Cloncurry was severely impacted, where, after experiencing 43 consecutive days above 40 °C from 16 December to 27 January (Bureau of Meteorology, 2019a), maximum temperatures fell below 24.5 °C for three straight days (3-5 February), with anomalies dropping to -12 °C. For minimum temperature anomalies, the conditions were not quite as extreme with average anomalies only falling to -2 °C (Supplementary Fig. S3),

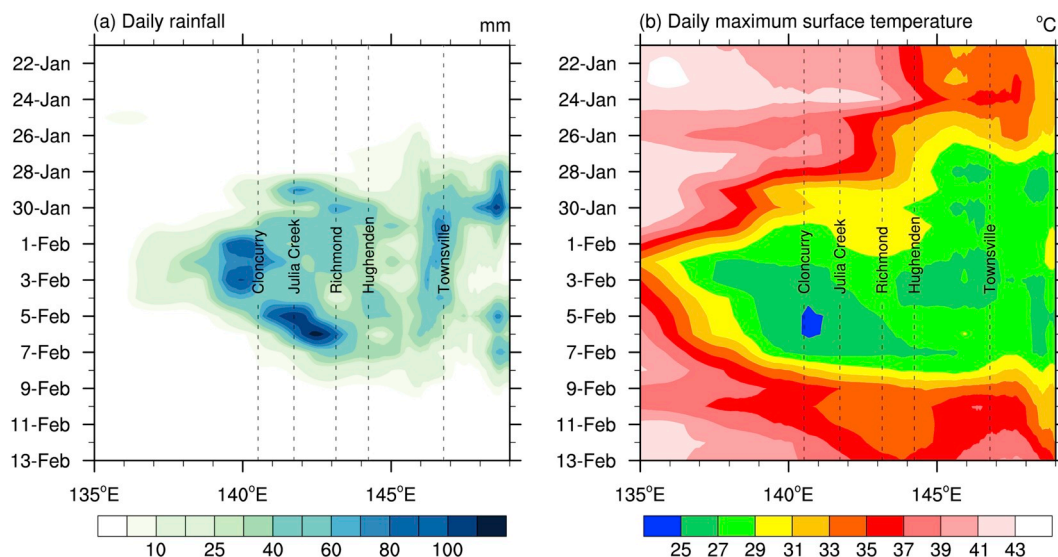


Fig. 5. (a) Daily rainfall and (b) daily maximum temperature, averaged over 18°-22°S, for 21 January to 13 February 2019. Both quantities are calculated from the gridded analysis data. The locations of five northern Queensland towns/cities are indicated by the vertical dashed lines. Winton (not shown) is located at a similar longitude to Richmond.

slightly west of the maximum temperature anomaly centre. Compounding the impacts of the low maximum temperatures and high rainfall totals were the anomalously high windspeeds (Supplementary Tables S1 and S2; Fig. S2). These produced a strong wind-chill factor with morning and afternoon apparent temperatures over Cloncurry and Julia Creek falling below 20 °C from the 3-6 February (Fig. 2c and d). Likewise, on 6 February, the 9am apparent temperature at Winton dipped to 16 °C (Fig. 2g), with six consecutive mornings of apparent temperatures below 22 °C (Fig. 2g). Richmond also experienced five mornings of apparent temperatures below 22 °C (Fig. 2e). This helps to confirm anecdotal evidence from graziers in the Julia Creek region that many cattle perished due to hypothermia brought on by the wind chill (M. Munchenberg, Pers. Comms.). However, we note that the apparent temperature calculation of Steadman (1994) was derived using the heat balance of the human body, not cattle, and it is likely that cattle standing in mud with wet coats experienced even greater heat losses and stress than indicated by these temperatures (Ferguson et al., 2008). The relatively cold conditions where maximum temperatures fell below 27 °C

extended from 1 February (east coast) to 7 February (inland Gulf stations), after which temperatures rapidly rose to above 31 °C from 8 February (Fig. 5b) as the monsoon depression weakened and migrated eastwards.

3.2. Associated meteorology and climate drivers acting during the event

The atmospheric conditions leading up to the flood featured an anomalous blocking anticyclone off the eastern Australian coast and Tropical Cyclone Riley situated off northwest Australia (Fig. 6, top two rows). Tropical Cyclone Riley developed as a tropical low on 21 January near 9°S, 128°E, and became a Category 1 storm on 24 January, peaking at Category 3 on 26 January. A second low pressure anomaly developed over Cape York during 23 - 27 January and over the following week it strengthened and gradually tracked southwards over Queensland's Gulf Country, drawing in moist air from the Coral Sea (Fig. 6, second row). It was this monsoon depression interacting with the wider atmospheric conditions, that directly caused the flooding event. As Tropical Cyclone

5-day average MSLP, wind anomalies (19-23 Jan to 7-11 Feb 2019)

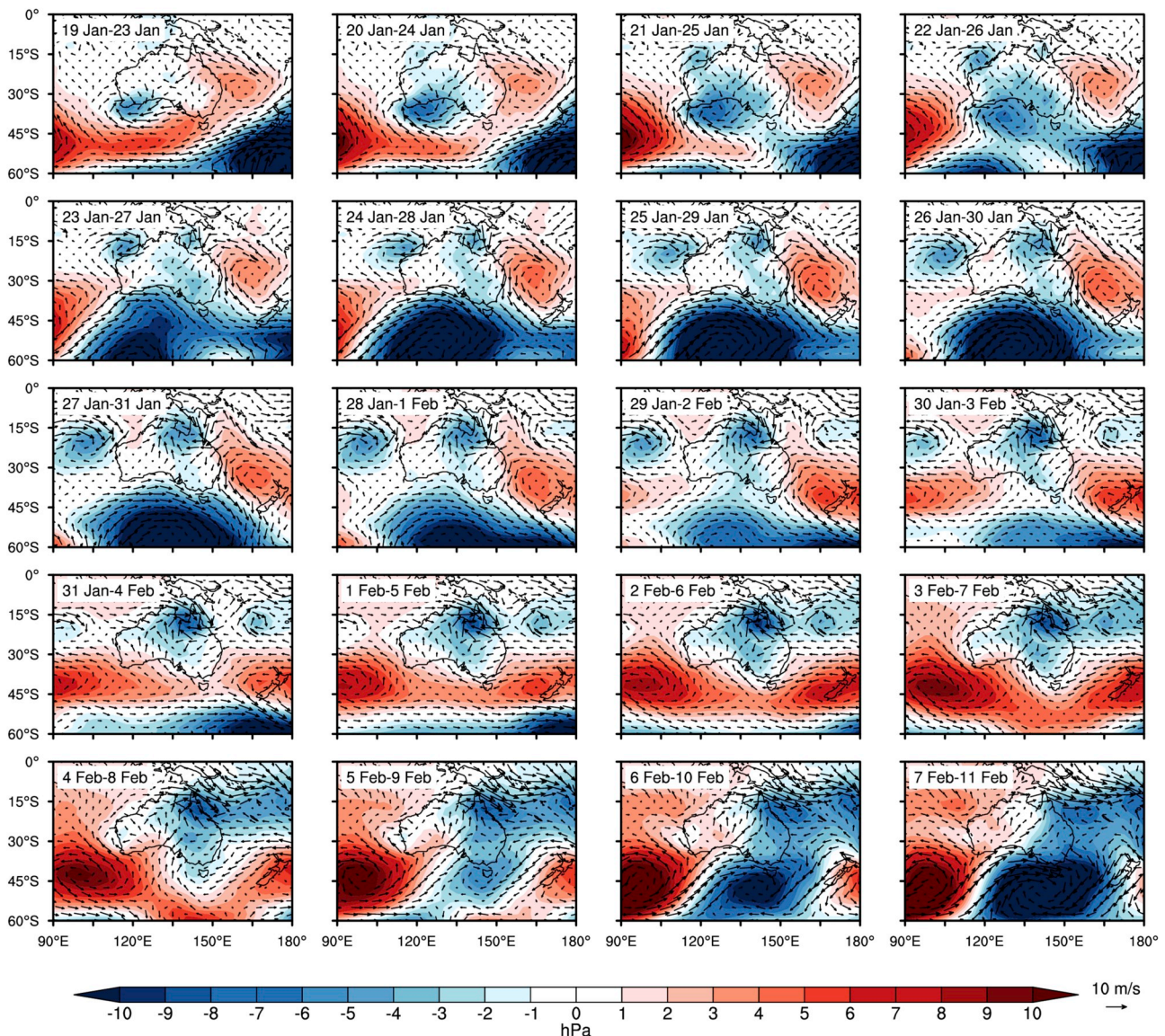


Fig. 6. Mean sea level pressure (MSLP) and near-surface (sigma level 995) daily wind anomalies, averaged over 5-day periods, from 19 –23 January to 7 –11 February. The order is from left to right, top to bottom.

Riley moved westwards from 31 January, the near-stationary monsoon depression over Queensland further intensified, forming a broad monsoon trough across the tropical north (Fig. 6, second and third rows). At about the same time, the anomalous anticyclone slowly shifted southeastwards towards New Zealand, helping to maintain the prominent easterly onshore flow onto the Queensland coast (Fig. 6, third and fourth rows). It was the near stationarity of the combined monsoon depression over Queensland and the anomalous anticyclone to its southeast, that appear to be the most important meteorological features of this event. Archived synoptic maps of the event can be viewed under the Bureau's Analysis Chart Archive page: <http://www.bom.gov.au/australia/charts/archive/index.shtml> (last accessed 14/08/2019).

We next focus on the role of the large-scale climate drivers for the event, and if they provided any pre-warning. These include the large-scale interannual tropical climate modes: the El Niño-Southern Oscillation (ENSO) and Indian Ocean Dipole (IOD), an intra-seasonal climate mode: the Madden-Julian Oscillation (MJO), and climate drivers whose origins lie in the extratropics and midlatitudes, respectively: the Southern Annular Mode (SAM) and atmospheric blocking. We also briefly discuss the role of westward propagating equatorial waves.

ENSO is arguably the most important climate driver for Australia (Nicholls et al., 1997), where historically, the association of Australian summer rainfall to ENSO has been for increased rainfall in northern and eastern Australia during La Niña (Risbey et al., 2009). Extreme rainfall over northern Queensland is more associated with La Niña or neutral conditions in the equatorial Pacific (Boschat et al., 2014), partly because there are higher tropical cyclone numbers along the northeast Queensland coast during La Niña summers (Kuleshov et al., 2008). However, the February 2019 floods developed during neutral to weak El-Niño conditions in the equatorial Pacific Ocean (Bureau of Meteorology, 2019b; https://www.cpc.ncep.noaa.gov/products/CDB/CDB_Archive.html/bulletin_012019/Tropics; last accessed 30/05/2019). This helps explain why the monthly rainfall outlook for February 2019 was for mostly dry or near-normal conditions across northern Australia (Fig. 4). ENSO can therefore be mostly ruled out as a contributing factor for this event, and it did not provide any capacity for advanced warning. Likewise, the IOD can be ruled out as a driver of this event given it is phase locked to the austral winter and spring seasons, and typically terminates by November (Risbey et al., 2009). Consistent with this, the IOD index, defined as the difference in sea surface temperature anomalies between the eastern and western tropical Indian Ocean, was near zero in January 2019.

The MJO is an intra-seasonal climate driver that has been shown to have a relatively strong association with northern Australian rainfall, especially in austral summer (Risbey et al., 2009). Historically, when the tropical convection of the MJO is located around the eastern Maritime Continent and western Pacific in summer, there is an increased chance of highest tercile rainfall over northern Australia (Wheeler et al., 2009). Based on the Real-time Multivariate MJO index (Wheeler and Hendon, 2004), the MJO was in phases 6 and 7 from 25 January to 11 February (pink lines in Fig. 7b), which are the phases typically associated with increased rainfall in far northern Queensland (Wheeler et al., 2009). The MJO is therefore able to at least partially explain the occurrence of this event, and it seems likely that the relatively long period of time for which the MJO was in phases 6 and 7 further helped the multi-day stationarity of the monsoon depression. As the predictability provided by the MJO is up to 3 weeks (Marshall and Hendon, 2019; Rashid et al., 2011) this suggests that it could have provided some advanced warning of the event. An analysis of MJO index forecasts from four dynamical prediction systems that were available on 23 January showed relatively good agreement that the MJO would be in phases 6 and 7 during the flood event (not shown). Before 20 January, however, the MJO forecasts were not in agreement (not shown).

The SAM, which describes the north-south shifts in atmospheric circulation (e.g., zonal wind and MSLP) in the mid- and high latitudes of the Southern Hemisphere, is an important climate driver for eastern

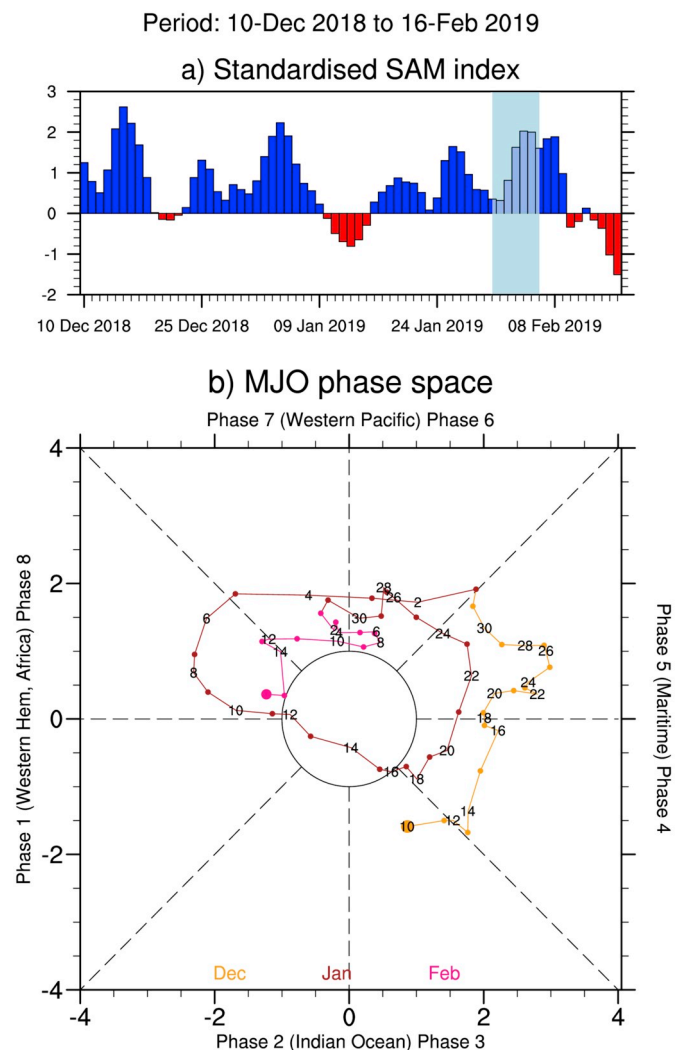


Fig. 7. (a) Daily standardised SAM index for 10 December 2018 to 16 February 2019, calculated by regressing the daily 700 hPa geopotential height (Z700) anomalies on to the leading EOF mode of monthly mean Z700 over 1979–2000. The SAM index is standardised by the standard deviation of the monthly SAM. Dark blue indicates positive values, while the light blue shading indicates when the week-long flooding event occurred. (b) MJO phase space diagram over the same period, with dots or numbers reflecting each day. The northern Queensland floods occurred when the MJO was in phases 6 and 7. (For interpretation of the references to colour in this figure legend, the reader is referred to the Web version of this article.)

Australia (Marshall et al., 2014). As shown by Hendon et al. (2007), the positive phase of the SAM typically sees anomalously high surface pressures near New Zealand and to the southwest of Australia, much like the pattern seen in the fourth row of Fig. 6. Indeed, positive SAM index values were a common feature from mid-December 2018 through to early February 2019 (Fig. 7a). Historically, there is a tendency for positive SAM phases to be associated with moist onshore easterly flow and rainfall reaching south-eastern Australia in summer, with an increased likelihood of upper quintile rainfall events stretching into central Queensland (Hendon et al., 2007). Therefore, this positive phase of the SAM may have partly contributed this extreme rainfall event. But as the predictability of the SAM is generally less than that of the MJO (Marshall et al., 2012) and its impacts are typically further south (Hendon et al., 2007), any prior warning that may have been available from the SAM was limited, especially since the SAM showed equally strong positive values during December and January (Fig. 7a).

As discussed above, the blocking anticyclone that occurred east of

Australia during the event appeared to play a role in bringing moist easterlies to the east coast of Queensland. Historically, Tasman Sea blocking anticyclones that form near the subtropical high ridge (39°S–40°S; Timbal and Drosowsky, 2013) coincide with a reduced probability of extreme heat across southeast Queensland (Marshall et al., 2014) and more extreme summer rainfall events across southern Queensland (Boschat et al., 2014). However, the region that was impacted by the February 2019 flooding and cold temperatures is further north than these typically-affected areas. Furthermore, the most-commonly used blocking index for Australia, that describes the

split of the westerly jet into a subtropical and polar component, is not suited for blocking centred at latitudes outside of 30°S to 55°S (Grose et al., 2012; Cowan et al., 2013), whereas the blocking anticyclone of this event was centred further north near 27°S. So, while the previous studies of Tasman Sea blocking cannot provide verification of its role in this event, it appears likely that the blocking anticyclone contributed to this event.

Another potential driving factor was the presence of an equatorial Rossby wave during late January and early February to the northeast of Queensland. These convectively coupled disturbances are westward

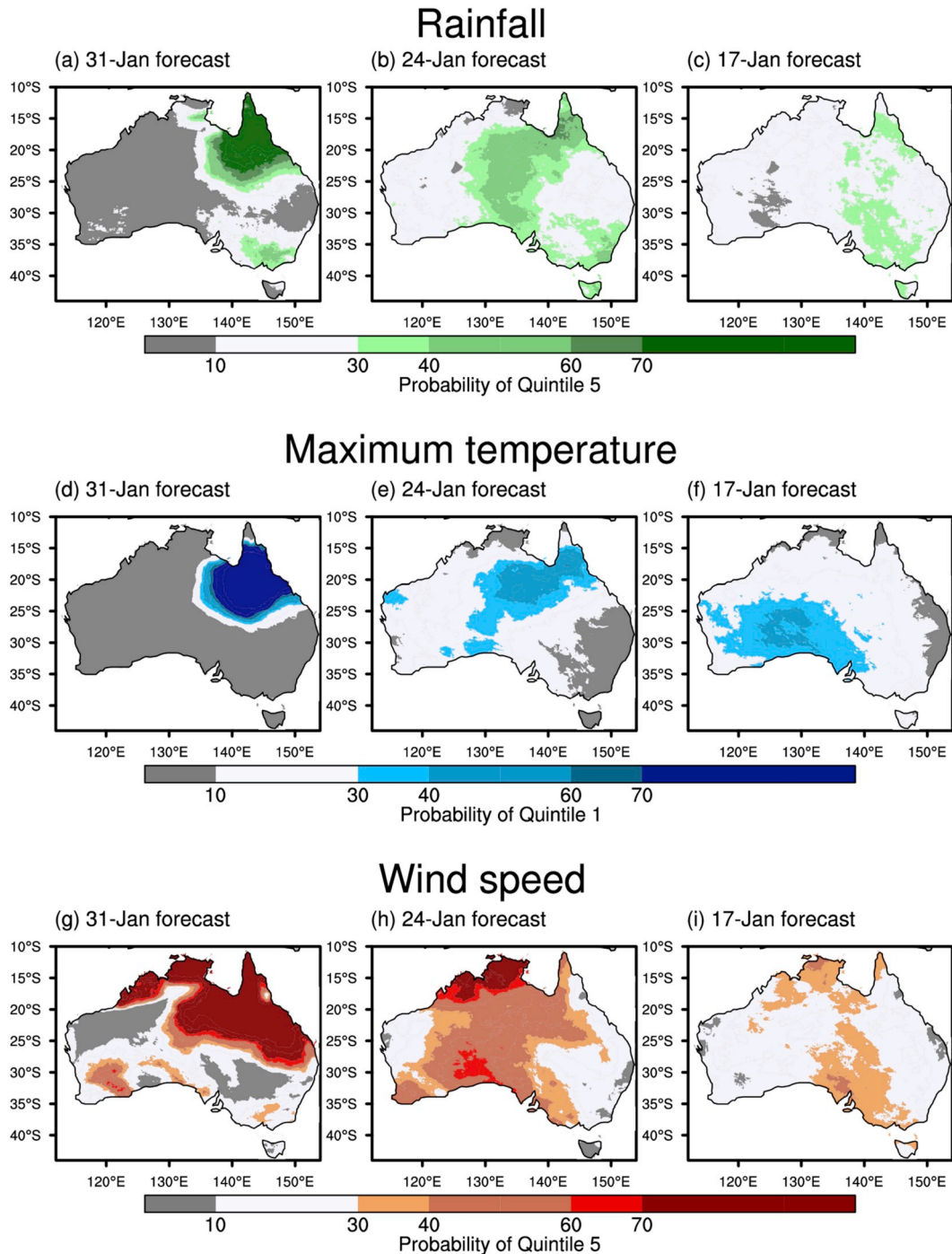


Fig. 8. ACCESS-S1 forecasts targeted to the week of 31 January to 6 February, from 31 January (i.e. week 1, left column), 24 January (i.e. week 2, middle column), and 17 January (i.e. week 3, right column), of the likelihood of (a-c) quintile 5 rainfall, (d-f) quintile 1 maximum temperatures, and (g-i) quintile 5 wind speeds. Quintile 5 rainfall and wind speeds refer to the wettest and windiest fifth of all historical weeks for that time of year, while quintile 1 Tmax refer to the coolest fifth of all historical weeks for that time of year.

propagating, with the $n=1$ wave symmetrical about the equator (Wheeler and Kiladis, 1999; Wheeler and Nguyen, 2015). On close inspection, however, the westward propagating OLR anomalies at the time and longitude of the event were positive, indicating a dry phase of the equatorial Rossby wave in this region (not shown), and hence ruling it out as a driver of this event.

To summarise the above, the most important potential large-scale drivers of this event appear to have been the MJO, the northward-shifted blocking anticyclone, and the SAM, but not ENSO or the IOD. Knowing this suggests that predictability of this event should potentially exist on the multi-week time scale, but not extend beyond the predictability of the MJO, since it is more predictable than blocking or the SAM.

3.3. ACCESS-S1 forecasts of the extreme conditions

As described in the introduction and presented in Fig. 4, the monthly rainfall outlook generated from the ACCESS-S1 system and issued to the public on 31 January for the month of February provided little indication of the extreme event. Yet, this monthly outlook was based on a 99-member forecast ensemble from 26 January that included model runs initialised up to 8 days prior (see Section 2.2). This embedded lag in the forecast ensemble is important to note, as it means that some of the ensemble members had a longer forecast lead and likely poorer skill. Here we examine whether multi-week forecasts of the probability of extreme conditions for the peak week, that were produced but not publicly issued, could have been more successful, especially if they could have been publicly released more quickly than was current practice for the monthly forecasts at that time.

Maps of forecast probabilities of the highest or lowest quintiles, of rainfall, temperature, and wind speed, are shown in Fig. 8. For the week 1 rainfall forecast, using initial conditions up to 31 January (i.e. comprising a total of 99 members initialised from 29–31 January, see Section 2.2), there was a forecast of a greater than 70% chance of rainfall being in the highest quintile for the whole of the flooded region (Fig. 8a). This represents a more than tripling of the climatological reference probability of 20% and was therefore quite a successful prediction. Just as successful were the week 1 forecasts of lowest quintile maximum temperature (Fig. 8d) and highest quintile windspeed (Fig. 8g). Although the 31 January forecast provides no lead time for the target week, it was still several days before the worst of the conditions were felt across northwest Queensland (Figs. 1 and 2, right side).

We now examine the week 2 forecasts that use initial conditions up to 24 January (middle column, Fig. 8). In comparison to the week 1 forecasts, they are less emphatic, but still highlight a much-increased chance of an extreme event. For rainfall, the forecast probability for the upper quintile in the affected region is in the range of 40–70% (Fig. 8b), still representing more than a doubling of the climatological probability. For maximum temperature (Fig. 8e) and windspeed (Fig. 8h), however, the forecast probabilities of the quintile extremes are slightly less at only 30–60% in the affected region, but still representing a much-increased likelihood compared to the 20% climatology.

Looking now at the week 3 forecasts (Fig. 8, right column), we see that the forecast probabilities are now much reduced in the region of interest, and therefore provided little indication of the event. In particular, the areas of Australia with the highest probabilities of the lowest quintile maximum temperature are now far removed from the region that experienced such low maximum temperatures (compare with Fig. 2b). Similarly, the windspeed forecast provided no indication that there would be extreme winds in the region of interest, and the rainfall forecast was far from emphatic. It appears that between 17–24 January the ability of the model to predict the event changed rapidly. This is consistent with the result reported above that the international models did not consistently forecast the future evolution of the MJO for forecasts initialised before about 20 January. This provides an understanding as to why the ACCESS-S1 monthly outlook for February (Fig. 4) did not predict a much increased chance of high rainfall, as two-thirds of

the aggregated 99-member lagged ensemble were initialised before 24 January (i.e., the outlook consisted of 11 runs per day from 18–26 January), beyond the apparent predictability of this event.

An alternative analysis showing the forecast probabilities for all the quintile categories for five northwest Queensland locations (see Table 1 for stations) is provided in Fig. 9. Shown are the week 2 forecasts from 24 January for the target peak week. For Cloncurry and Julia Creek, the highest quintile probabilities sit at 48% and 43%, respectively (Fig. 9a, c), which represents more than a doubling of the climatological likelihood of extreme rainfall for the peak week. For the three stations (Richmond, Hughenden, Winton) that were furthest away from the observed rainfall maxima centre, their forecasts show a more equal spread across the quintiles, with the percentage range of 27–30% falling in the highest quintile bin (Fig. 9e, g, i). For maximum temperature, Cloncurry had a forecast probability of 48% for the lowest quintile, compared to 38% for Julia Creek (Fig. 9b, d). This accurately represents where the coldest anomalies were observed, just south of Cloncurry. The lower probabilities of the lowest quintile temperature in Richmond, Hughenden and Winton (range of 29–32%; Fig. 9f, h, j) reflects the fact that the ACCESS-S1 forecast placed a higher likelihood of colder temperatures (and extreme rainfall) too far west (Fig. 8e).

3.4. ACCESS-S1 forecasts of the large-scale atmosphere

Fig. 10 compares the ensemble forecast, initialised on 24 January, of global-scale anomalous MSLP, 850 hPa zonal wind and OLR with observed and reanalysis patterns for the event's peak week. For MSLP anomalies, ACCESS-S1 skilfully predicted the anomalous surface pressure ridge to the south of Australia, including the anomaly centres to the south of Africa and west of southern South America (Fig. 10a and b). The forecast shows a broad-scale low pressure anomaly centre over Australia that stretches from the Northern Territory through to northern Victoria. In the reanalysis, the monsoon depression is fixed on the Gulf of Carpentaria and linked to a broad monsoon trough that extends out into the western Pacific (Fig. 10b). The model captures strong westerly anomalies across Cape York and the Top End, with somewhat weaker anomalous easterlies, south of approximately 20°S extending down into Tasmania (Fig. 10c), yet struggles to predict the intense easterly anomaly centre between 140°E and 150°E, centred at 20°S (Fig. 10d). It was this strong easterly component that helped trigger the relatively cold wind chill temperatures around the pastoral districts of Julia Creek and Cloncurry (see temperatures in Fig. 2). These strong easterly anomalies were better forecast in the week 1 forecast (from 31 January) because, at this time, ACCESS-S1 was predicting the correct position of the monsoon depression over the Gulf when averaged over the peak week (not shown).

For OLR, the ACCESS-S1 forecasts were quite accurate over the Indo-Pacific, with negative OLR anomalies (increased cloudiness) over northern Queensland, and positive OLR anomalies (reduced cloudiness) over northwest Australia stretching into the Sumatra-Java region (Fig. 10e). This pattern is typical of an active MJO in phases 6 to 7 at that time of year (Wheeler et al., 2009), as was observed (Fig. 7b). Just perceptible in the observed OLR are the two grid-scale negative centres over northern Queensland, one centred near Townsville and one in the Flinders River region (Fig. 10f). The ACCESS-S1 ensemble manages to capture these features in its 25 January forecast for the week of 25 January–31 January (not shown), however this ability does not extend beyond the one-week lead-time. The OLR and zonal wind forecasts are consistent with the enhanced convective phase of the MJO over the western tropical Pacific and north-eastern Australia, and we can summarise by saying that the broad-scale atmospheric conditions were well forecast a week prior to the event.

24-Jan forecast for 31-Jan to 6-Feb

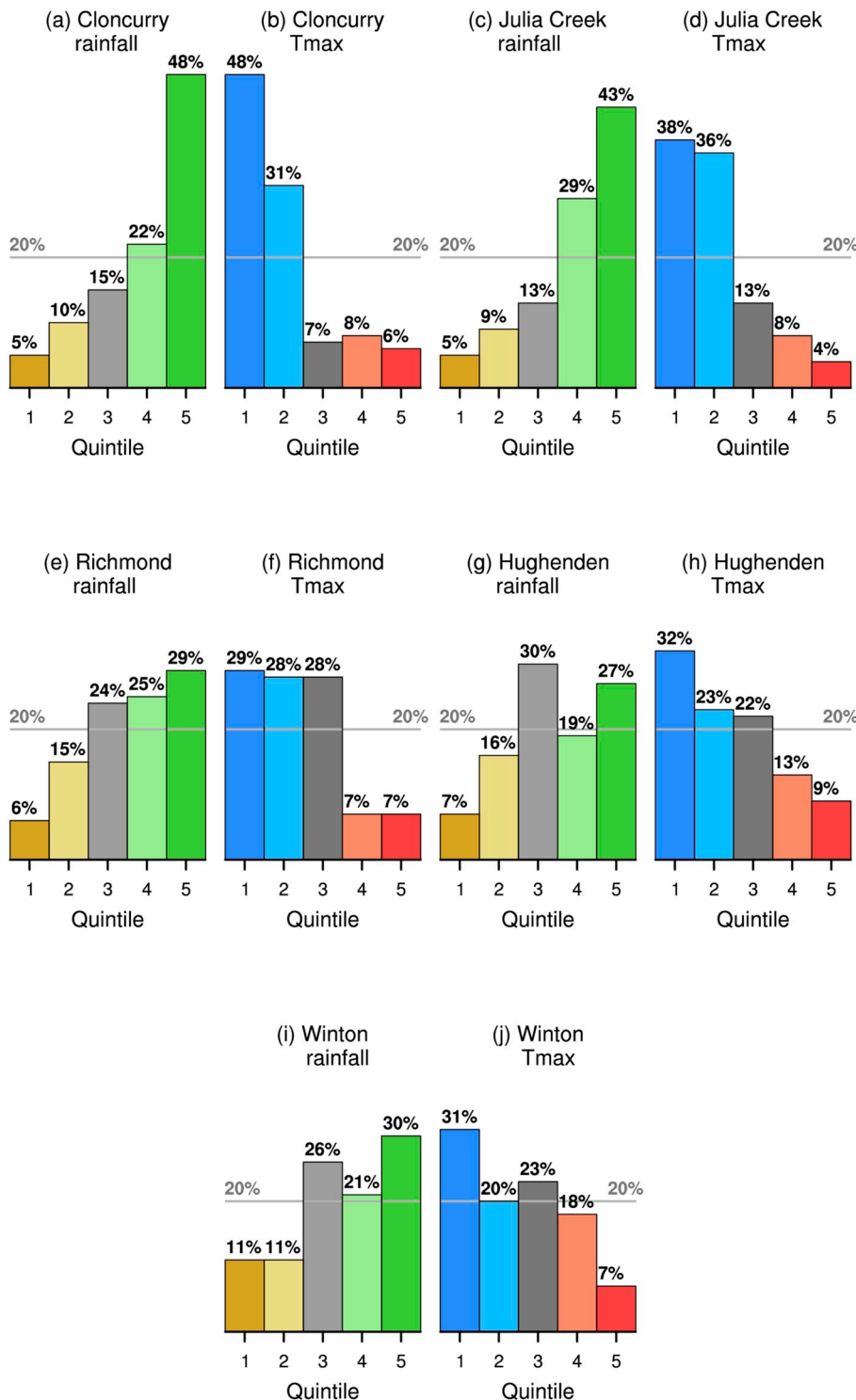


Fig. 9. The percentage of 24 January forecasts of rainfall and maximum temperatures for the week of 31 January to 6 February that fall into each quintile based on historical observations from 1990 to 2012. Shown are forecasts for a 5 km grid cell that encompasses Bureau observational stations near (a, b) Cloncurry, (c, d) Julia Creek, (e, f) Richmond, (g, h) Hughenden, and (i, j) Winton (Table 1 for stations used). The 20% climatological reference likelihood is shown by the grey line. The average observed rainfall and maximum temperatures for 31 January to 6 February week fell into the highest and lowest quintiles, respectively.

3.5. Comparing the ensemble mean and members with other S2S prediction systems

Here we compare the rainfall accumulation forecasts from ACCESS-S1 against four international S2S prediction systems (see Methods for details). As with the previous section, we use forecasts initialised on 24 January, focusing on the accumulated rainfall for the peak week. The

ACCESS-S1 ensemble mean produced amounts of between 50 and 150 mm over northwest Queensland, and totals in excess of 200 mm along the coastal strip encompassing Townsville (Fig. 11a). As previously described, the observed rainfall totals for these regions far exceeded 400 mm during the peak week (Fig. 11f). Both the ECMWF and Météo-France ensemble mean forecasts of rainfall totals were between 100 and 150 mm over northwest Queensland (Fig. 11b and c), however

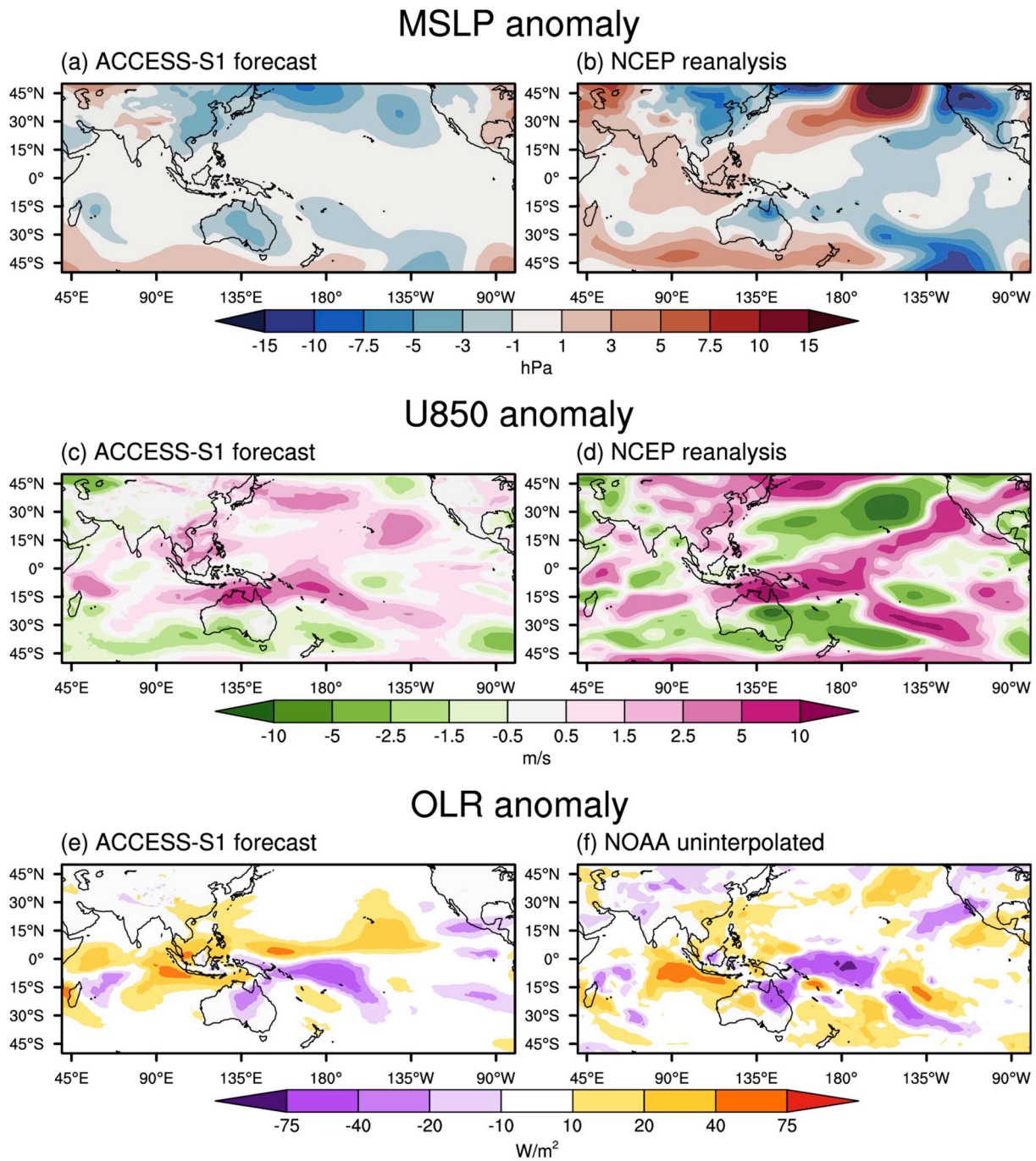


Fig. 10. (left) ACCESS-S1 ensemble forecasts for the week of 31 January to 6 February of (a) MSLP anomaly, (c) 850 hPa westerly wind anomaly, and (e) outgoing long wave radiation anomaly. Forecasts are initialised between 22 - 24 January. (right) reanalysis anomalies of (b) MSLP, (d) 850 hPa westerly winds and (f) observed OLR. All anomalies are calculated with respect to a 1990-2012 climatology.

as with ACCESS-S1, they place the maximum rainfall too far north and west, stretching into the Northern Territory. Interestingly, both the ECMWF and ACCESS-S1 systems predict greater rainfall totals (100–150 mm) along the coast to the north of Townsville, while the Météo-France prediction is quite localised to Townsville. The remaining two systems (NCEP and POAMA) forecast ensemble mean rainfall totals of 150–200 mm for the far north of Cape York and into the Arafura Sea (Fig. 11d and e). This type of rainfall pattern is more typically aligned with an active MJO in phases 6 to 7 for that time of year (e.g., Wheeler et al., 2009). Both NCEP and POAMA’s accumulated rainfall patterns are overly zonal and diminish over the inland Gulf region. The ensemble mean from these two systems only predict less than 25 mm of rainfall in

total for the event week over northwest Queensland, quite a substantial under-prediction.

Delving deeper into the individual ensemble members, we find that ACCESS-S1 gets closest to the observed magnitude, with one of its 99 members forecasting just over 410 mm for the most heavily impacted area of northwest Queensland (140°-142°E, 19°-21°S; Fig. 12a; the observed areal average was 518 mm). This member captures the correct position of the monsoon depression during this week and the associated strong easterlies, although over-estimates the cloudiness as represented by large negative OLR anomalies (Supplementary Fig. S4). It is worth noting that two other individual ACCESS-S1 members forecast 861 mm and 775 mm, respectively, for Townsville, compared to an observed

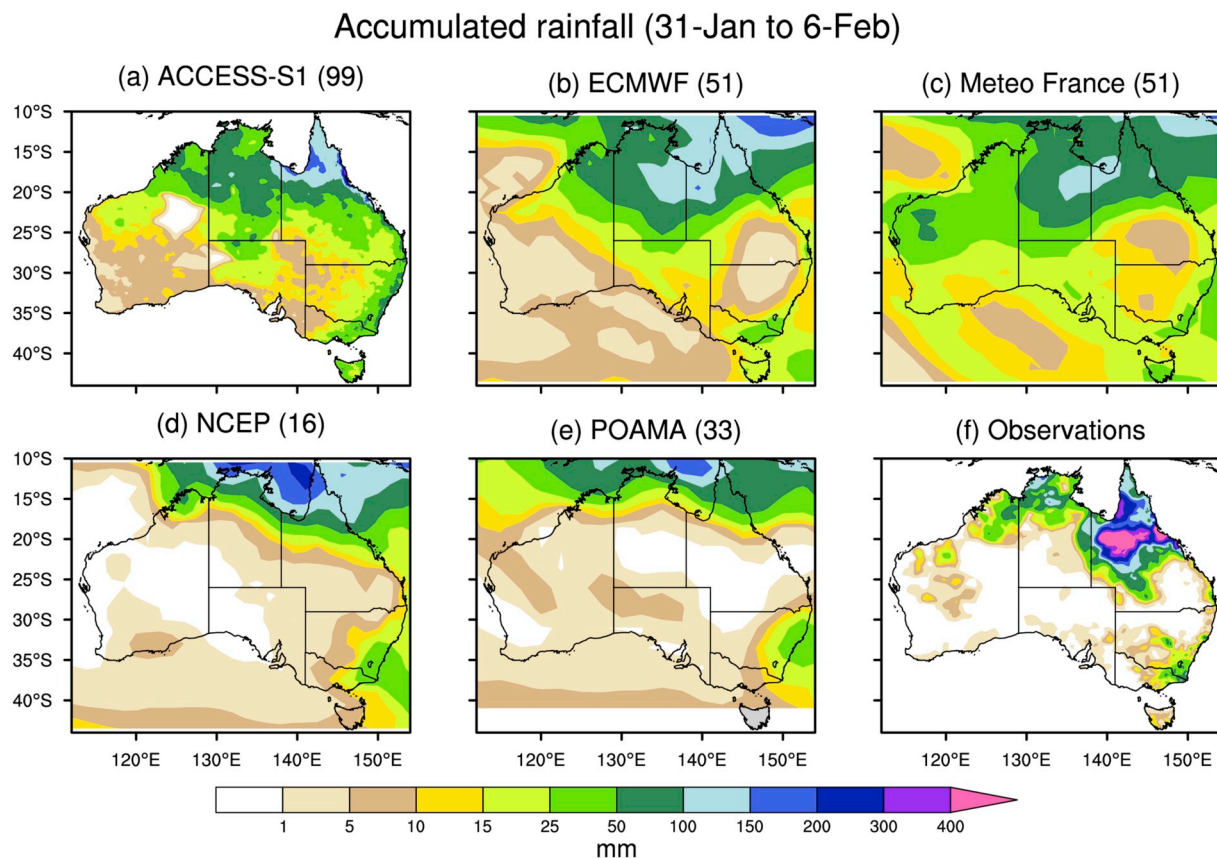


Fig. 11. Accumulated ensemble-mean rainfall forecasts for the week of 31 January to 6 February, as initialised on 24 January from (a) ACCESS-S1, (b) ECMWF, (c) POAMA, (d) NCEP and (e) Météo-France. The number of ensemble members is shown in the parentheses. (f) Observed accumulated rainfall for the same week. Note, that 99 members of ACCESS-S1 were each initialised between 22 - 24 January (i.e., 33 members on each day).

areal average of 679 mm (not shown). In all, 13 of its 99 members forecast totals of over 200 mm for the boxed region in Fig. 12a. Individual members from ECMWF perform equally well, with 8 out of 51 members forecasting totals over 200 mm for northwest Queensland, respectively, with the largest magnitude forecasts for each region both exceeding 330 mm (Fig. 12b; note that totals exceed 400 mm just west of Cloncurry). The Météo-France system under-forecasts the rainfall in all of its 51 members, with only one member forecasting over 200 mm (Fig. 12c). Both NCEP and POAMA members significantly underestimate the accumulated rainfall in both regions (Fig. 12d, e), each seemingly struggling to forecast the observed totals inland of the Gulf of Carpentaria. Reasons for the discrepancy between the ability of the different S2S prediction systems to produce good-performing individual members might be due to: (a) the different model resolutions; (b) the different ensemble sizes; (c) the different initial conditions and perturbation strategies; (d) the forecast calibration or lack thereof; and (e) the general model performance. Further work will be required to determine if the best-performing ensemble members of the other S2S systems had similar synoptic patterns, such as the quasi-stationary monsoon depression and northern Tasman Sea blocking anticyclone in the preceding weeks.

4. Discussion and conclusions

This study has shown that the extreme wet, windy and cold conditions over northern Queensland that extended through late January to early February 2019, and resulted in an estimated 625,000 cattle deaths, were caused by a quasi-stationary monsoon depression. While some cattle deaths were attributed to flooding (drowning), unusually low maximum temperatures and strong winds were significant factors, with many cattle dying due to exposure. Adding to this, the heat wave

conditions across the north during December and January (Bureau of Meteorology, 2019a) and ongoing multi-year drought most likely compounded the malnourishment of cattle prior to the flooding. Further research is therefore warranted on quantifying the roles that the extreme weather conditions, preceding heat and drought played in the high cattle mortality rates.

We have shown that the monsoon depression coincided with an active MJO pulse with enhanced convection lingering in the western Pacific and over north-eastern Australia for around two weeks, against the backdrop of weak El Niño conditions in the equatorial Pacific. In contrast, in early January an MJO pulse propagated across the western Pacific in only 5 days, indicative of the MJO's large temporal variability. A westward propagating equatorial Rossby wave was present during the lead-up to the event, however it was in a dry/suppressed phase, and hence unlikely to have contributed to the floods. A positive SAM phase, along with a blocking anticyclone in the northern Tasman Sea, just north of the climatological subtropical high ridge position in February, led to strong anomalous easterlies along the northern Queensland coast prior to, and during, the peak week of the flood and may have contributed to the extreme nature of the event. It is not unusual for the MJO to stall in its eastward propagation (Kim et al., 2014), however there is limited understanding as to why this occurs. The role of local and remote sea surface temperatures in promoting convection associated with the monsoon depression may have been a factor, given that an MJO event in March 2015 was amplified by anomalously warm temperatures in the central Pacific during the development of an El Niño (Marshall et al., 2016). We further highlighted the presence of a northern Tasman Sea anticyclone in the leading weeks, however the extent to which this anticyclone and mid-latitude interactions played a role in the stationarity of the monsoon depression is subject to ongoing investigation.

Accumulated rainfall (31-Jan to 6-Feb); highest rainfall predictions over NW Qld

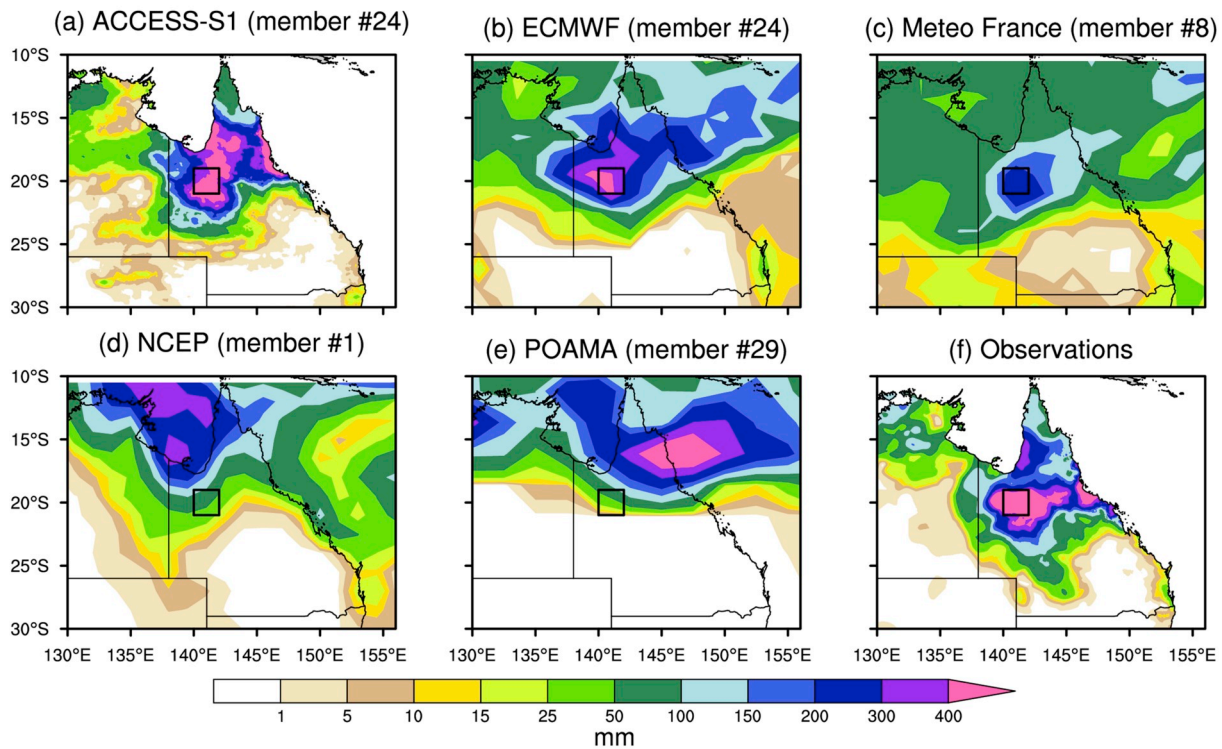


Fig. 12. As in Fig. 11, but for individual ensemble members that forecast the highest weekly accumulated rainfall over northwest Queensland (box encompassing 140°–142°E, 19°–21°S), over which the rainfall totals were averaged to identify the individual model members.

This study demonstrates that the weather conditions associated with this flooding event were not well-predicted beyond two weeks with current state-of-the-art forecasting systems. Yet the prototype weekly forecasts derived from a 99-member ACCESS-S1 ensemble, initialised on 24 January, predicted a 40–60% probability of extreme rainfall, cold temperatures and high winds for the week ending on 6 February over northern Queensland. From a risk perspective, this amounts to a doubling of the likelihood of extreme conditions when referenced against climatology which can be viewed as a successful forecast. This forecast placed the extreme rainfall slightly north of where the worst impacts were felt. While ACCESS-S1 showed good skill at predicting the large-scale convection around north-eastern Australia, as well as the band of strong westerlies over northern Australia, it greatly underestimated the easterlies. Consistent with other international forecast systems, the ACCESS-S1 ensemble-mean significantly underestimated the magnitude and spatial extent of the rainfall associated with the monsoon depression. Despite this, ACCESS-S1 was the only system to have an ensemble member close to the observed for accumulated rainfall for the peak week over the northwest (on a side note, ACCESS-S1 had two members that captured more than the observed rainfall over Townsville; not shown). This member successfully captured the position of the monsoon depression as well the location and strength of the easterlies. The next step will be to understand why most of the ensemble members under-forecast the event's rainfall magnitude and if it relates to their simulation of the monsoon depression, its magnitude and trajectory, and relevant climate and weather drivers. Does this indicate a systematic bias in forecast systems (e.g., a failure to adequately represent certain physical processes) or it is just a case that the event was overly complex in its dynamics making it inherently unpredictable beyond two weeks? There is potential to increase the skill in ACCESS-S1 (and the successor S2) forecasts as our understanding of the prediction system's deficiencies grows. This will undoubtedly lead to improved

forecasts, particularly on the multi-week timescale, critically important for agriculture and grazing across northern Australia.

What this study has demonstrated is the potential benefit of multi-week forecasts, even though these types of extremes forecast products are currently unavailable to the wider community. Reflecting a first step towards seamless prediction, the Bureau of Meteorology began issuing multi-week forecasts in late August 2019, that show the chance of above median rainfall and temperature (released on a weekly basis). Yet in January 2019, graziers and other users had to rely on monthly outlooks issued on a fortnightly basis that included only rainfall, and minimum and maximum temperature – with the outlooks showing chance of above the median. As we have noted, the monthly rainfall outlook for February 2019, published online on 31 January (Fig. 4), was produced using the model runs initialised from 18–26 January (i.e., using runs up to 13 days before being published), and therefore its skill was compromised by being delayed and not focused on the peak flooding week. The benefits of multi-week forecasts shown in this study are that they potentially only include forecasts initialised up to 3 days earlier, and they are better able to discriminate extreme events that last for about a week.

As to whether the release of multi-week forecasts would have dramatically changed the outcomes that graziers and producers experienced across northwest Queensland is an open question. If the multi-week outlooks had been publicly available, then an extra few days of warning may have made a sizeable difference to some producers. As one Julia Creek grazier has suggested, what is required in the future is a 3–5 day lead time with high confidence (D. Lynch, Pers. Comm.). What this study has demonstrated is that trial prototype products have the potential to fill in the multi-week prediction gap between the day-to-day weather forecasts and the monthly-seasonal outlooks. Multi-week predictions of the probability of extreme conditions would directly benefit the agricultural sector, particularly in the case of products that provide location-specific information, as shown for specific localities over

northwest Queensland in this study.

Acknowledgements

We thank Vincent Villani for providing the satellite imagery in Fig. 3. We are deeply indebted to the ACCESS-S1 seasonal prediction team, particularly those who develop and maintain the prototype products, including Griffith Young, Hailin Yan, Harley Dallafiore and Debra Hudson. The funding is provided by Meat and Livestock Australia (MLA), the Queensland Government through the Drought and Climate Adaptation Program, and University of Southern Queensland through the Northern Australian Climate Program (NACP). The NACP is coordinated by Roger Stone. Catherine de Burgh-Day's contribution is part of the Forewarned is Forearmed project, which is supported by funding from the Australian Government Department of Agriculture as part of its Rural R&D for Profit program. The international forecast model results are based on data from the S2S project, a joint initiative of the World Weather Research Programme (WWRP) and the World Climate Research Programme (WCRP). The original S2S project database is hosted at ECMWF as an extension of the TIGGE database.

We thank the Hanh Nguyen, and the two external reviewers for providing constructive feedback on earlier drafts.

Appendix A. Supplementary data

Supplementary data to this article can be found online at <https://doi.org/10.1016/j.wace.2019.100232>.

References

- Boschat, G., Pezza, A., Simmonds, I., Perkins, S., Cowan, T., Purich, A., 2014. Large scale and sub-regional connections in the lead up to summer heat wave and extreme rainfall events in eastern Australia. *Clim. Dyn.* <https://doi.org/10.1007/s00382-014-2214-5>.
- Bureau of Meteorology, 2019. Special Climate Statement 68 — Widespread Heatwaves during December 2018 and January 2019. Bureau of Meteorology.
- Bureau of Meteorology, 2019. Special Climate Statement 69 — an Extended Period of Heavy Rainfall and Flooding in Tropical Queensland. Bureau of Meteorology.
- Cottrill, A., Hendon, H.H., Lim, E.-P., Langford, S., Shelton, K., Charles, A., McClymont, D., Jones, D., Kuleshov, Y., 2013. Seasonal Forecasting in the Pacific using the coupled model POAMA-2. *Weather Forecast.* 28, 668–680. <https://doi.org/10.1175/WAF-D-12-00072.1>.
- Cowan, T., Van Rensch, P., Purich, A., Cai, W., 2013. The association of tropical and extratropical climate modes to atmospheric blocking across southeastern Australia. *J. Clim.* 26, 7555–7569. <https://doi.org/10.1175/JCLI-D-12-00781.1>.
- Dee, D.P., Uppala, S.M., Simmons, A.J., Berrisford, P., Poli, P., Kobayashi, S., Andrae, U., Balmaseda, M.A., Balsamo, G., Bauer, P., Bechtold, P., Beljaars, A.C.M., Berg, L. Van De, Bidlot, J., Bormann, N., Delsol, C., Dragani, R., Fuentes, M., Geer, A.J., Haimberger, L., Healy, S.B., Hersbach, H., Holm, E.V., Isaksen, I., Kallberg, P., Kohler, M., Matricardi, M., McNally, A.P., Monge-Sanz, B.M., Morcrette, J.J., Park, B.K., Peubey, C., de Rosney, P., Tavolato, C., Thepaut, J.N., Vitart, F., 2011. The ERA-Interim reanalysis: configuration and performance of the data assimilation system. *Q. J. R. Meteorol. Soc.* 137, 553–597. <https://doi.org/10.1002/qj.828>.
- ECMWF, 2018. Part V: ensemble prediction system. In: IFS Documentation CY45R1. ECMWF.
- Ferguson, D., Colditz, I., Fisher, A., 2008. Animal Welfare Assessment in Cattle Feedlots – A Review. Meat & Livestock Australia Limited.
- Gissing, A., O'Brien, J., Hussein, S., Evans, J., Mortlock, T., 2019. Townsville 2019 flood – insights from the field. *Risk Front. Brief. Note* 389, 1–8.
- Grose, M.R., Pook, M.J., McIntosh, P.C., Risbey, J.S., Bindoff, N.L., 2012. The simulation of cutoff lows in a regional climate model: reliability and future trends. *Clim. Dyn.* 39, 445–459. <https://doi.org/10.1007/s00382-012-1368-2>.
- Hendon, H.H., Thompson, D.W.J., Wheeler, M.C., 2007. Australian rainfall and surface temperature variations associated with the Southern Hemisphere annular mode. *J. Clim.* 20, 2452–2467. <https://doi.org/10.1175/JCLI4134.1>.
- Hudson, D., Alves, O., Hendon, H.H., Lim, E., Luo, J., MacLachlan, C., Marshall, A.G., Shi, L., Wang, G., Wedd, R., Young, G., Zhao, M., Zhou, X., 2018. ACCESS-S1: the new Bureau of Meteorology multi-week to seasonal prediction system. *J. South. Hemisphere Earth Syst. Sci.* 67, 132–159. <https://doi.org/10.22499/3.6703.001>.
- Hudson, D., Marshall, A.G., Alves, O., Young, G., Jones, D., Watkin, A., 2016. Forewarned is forearmed: extended-range forecast guidance of recent extreme heat events in Australia. *Weather Forecast.* 31, 697–711. <https://doi.org/10.1175/WAF-D-15-0079.1>.
- Jeon, S., Paciorek, C.J., Wehner, M.F., 2016. Quantile-based bias correction and uncertainty quantification of extreme event attribution statements. *Weather Clim. Extrem.* 12, 24–32. <https://doi.org/10.1016/j.wace.2016.02.001>.
- Jones, D.A., Wang, W., Fawcett, R., 2009. High-quality spatial climate data-sets for Australia. *Aust. Meteorol. Oceanogr. J.* 58, 233–248.
- Kalnay, E., Kanamitsu, M., Kistler, R., Collins, W., Deaven, D., Gandin, L., Iredell, M., Saha, S., White, G., Woollen, J., Zhu, Y., Chelliah, M., Ebisuzaki, W., Higgins, W., Janowiak, J., Mo, K.C., Ropelewski, C., Wang, J., Leetmaa, A., Reynolds, R., Jenne, R., Joseph, D., 1996. The NCEP/NCAR 40-year reanalysis project. *Bull. Am. Meteorol. Soc.* 77, 437–472.
- Kim, D., Kug, J., Sobel, A.H., 2014. Propagating versus nonpropagating Madden-Julian oscillation events. *J. Clim.* 27, 111–125. <https://doi.org/10.1175/JCLI-D-13-00084.1>.
- Kuleshov, Y., Qi, L., Fawcett, R., Jones, D., 2008. On tropical cyclone activity in the Southern Hemisphere: Trends and the ENSO connection. *Geophys. Res. Lett.* 35. <https://doi.org/10.1029/2007GL032983>.
- MacLachlan, C., Arribas, A., Peterson, K.A., Maidens, A., Fereday, D., Scaife, A.A., Gordon, M., Vellinga, M., Williams, A., Comer, R.E., Camp, J., Xavier, P., Madec, G., 2015. Global Seasonal forecast system version 5 (GloSea5): a high-resolution seasonal forecast system. *Q. J. R. Meteorol. Soc.* 5, 1072–1084. <https://doi.org/10.1002/qj.2396>.
- Marshall, A.G., Hendon, H.H., 2019. Multi-week prediction of the Madden-Julian oscillation with ACCESS-S1. *Clim. Dyn.* 52, 2513–2528. <https://doi.org/10.1007/s00382-018-4272-6>.
- Marshall, A.G., Hendon, H.H., Wang, G., 2016. On the role of anomalous ocean surface temperatures for promoting the record Madden-Julian Oscillation in March 2015. *Geophys. Res. Lett.* 43, 472–481. <https://doi.org/10.1002/2015GL066984>.
- Marshall, A.G., Hudson, D., Wheeler, M.C., Alves, O., Hendon, H.H., Pook, M.J., Risbey, J.S., 2014. Intra-seasonal drivers of extreme heat over Australia in observations and POAMA-2. *Clim. Dyn.* 43, 1915–1937. <https://doi.org/10.1007/s00382-013-2016-1>.
- Marshall, A.G., Hudson, D., Wheeler, M.C., Hendon, H.H., Alves, O., 2012. Simulation and prediction of the Southern Annular Mode and its influence on Australian intra-seasonal climate in POAMA. *Clim. Dyn.* 38, 2483–2502. <https://doi.org/10.1007/s00382-011-1140-z>.
- Nicholls, N., Drosowsky, W., Lavery, B., 1997. Australian rainfall variability and change. *Weather* 52, 66–72. <https://doi.org/10.1002/j.1477-8696.1997.tb06274.x>.
- Rashid, H.A., Hendon, H.H., Wheeler, M.C., Alves, O., 2011. Prediction of the Madden-Julian oscillation with the POAMA dynamical prediction system. *Clim. Dyn.* 36, 649–661. <https://doi.org/10.1007/s00382-010-0754-x>.
- Risbey, J.S., Pook, M.J., McIntosh, P.C., Wheeler, M.C., Hendon, H.H., 2009. On the remote drivers of rainfall variability in Australia. *Mon. Weather Rev.* 137, 3233–3253. <https://doi.org/10.1175/2009MWR2861.1>.
- Saha, S., Moorthi, S., Wu, X., Wang, J., Nadiga, S., Tripp, P., Behringer, D., Hou, Y., Chuang, H., Iredell, M., Ek, M., Meng, J., Yang, R., Mendez, M.P., van den Dool, H., Zhang, Q., Wang, W., Chen, M., Becker, E., 2014. The NCEP climate forecast system version 2. *J. Clim.* 27, 2185–2208. <https://doi.org/10.1175/JCLI-D-12-00823.1>.
- Steadman, R.G., 1994. Norms of apparent temperature in Australia. *Aust. Meteorol. Mag.* 43, 1–16.
- Timbal, B., Drosowsky, W., 2013. The relationship between the decline of Southeastern Australian rainfall and the strengthening of the subtropical ridge. *Int. J. Climatol.* 33, 1021–1034. <https://doi.org/10.1002/joc.3492>.
- Vitart, F., Ardilouze, C., Bonet, A., Brookshaw, A., Chen, M., Codorean, C., Déqué, M., Ferranti, L., Fucile, E., Fuentes, M., Hendon, H., Hodgson, J., Kang, H., Kumar, A., Lin, H., Liu, G., Liu, X., Malguzzi, P., Mallas, I., Manoussakis, M., Mastrangelo, D., MacLachlan, C., McLean, P., Minami, A., Mladek, R., Nakazawa, T., Najm, S., Nie, Y., Rixen, M., Robertson, A.W., Ruti, P., Sun, C., Takaya, Y., Tolstykh, M., Venuti, F., Waliser, D., Woolnough, S., Wu, T., Won, D., Xiao, H., Zaripov, R., Zhang, L., 2017. The subseasonal to seasonal (S2S) prediction project database. *Bull. Am. Meteorol. Soc.* 98, 163–173. <https://doi.org/10.1175/BAMS-D-16-0017.1>.
- Voldoire, A., Sanchez-Gomez, E., Melia, D.S. y, Decharme, B., Cassou, C., Senesi, S., Valcke, S., Beau, I., Alias, A., Chevallier, M., Deque, M., Deshayes, J., Douville, H., Fernandez, E., Madec, G., Maiconnave, E., Moine, M.-P., Planton, S., Saint-Martin, D., Szopa, S., Tyteca, S., Alkama, R., Belamari, S., Braun, A., Coquart, L., Chauvin, F., 2013. The CNRM-CM5.1 global climate model: description and basic evaluation. *Clim. Dyn.* 40, 2091–2121.
- Wheeler, M., Kiladis, G.N., 1999. Convectively coupled equatorial waves: analysis of clouds and temperature in the wavenumber–frequency domain. *J. Atmos. Sci.* 56, 374–399. [https://doi.org/10.1175/1520-0469\(1999\)056<0374:ccewao>2.0.co;2](https://doi.org/10.1175/1520-0469(1999)056<0374:ccewao>2.0.co;2).
- Wheeler, M.C., Hendon, H.H., 2004. An all-season real-time multivariate MJO index: development of an index for monitoring and prediction. *Mon. Weather Rev.* 132, 1917–1932. [https://doi.org/10.1175/1520-0493\(2004\)132<1917:AARMMI>2.0.CO;2](https://doi.org/10.1175/1520-0493(2004)132<1917:AARMMI>2.0.CO;2).
- Wheeler, M.C., Hendon, H.H., Cleland, S., Meinke, H., Donald, A., 2009. Impacts of the Madden-Julian oscillation on Australian rainfall and circulation. *J. Clim.* 22, 1482–1498. <https://doi.org/10.1175/2008JCLI2595.1>.
- Wheeler, M.C., Nguyen, H., 2015. Equatorial waves. In: North, G.R., Pyle, J., Zhang, F. (Eds.), *Encyclopedia of Atmospheric Sciences*, pp. 102–112.